Title

Violent Quenching: Molecular Gas Blown to 1000 kms(-1) during a Major Merger

Journal

ASTROPHYSICAL JOURNAL LETTERS, 864(1)

ISSN

2041-8205

Authors

Geach, JE
Tremonti, C
Diamond-Stanic, AM
et al.

Publication Date

2018-09-01

DOI

10.3847/2041-8213/aad8b6

Peer reviewed

The Astrophysical Journal Letters, 864:L1 (6pp), 2018 September 1 https://doi.org/10.3847/2041-8213/aad8b6

Violent Quenching: Molecular Gas Blown to 1000 km s^{-1} during a Major Merger

J. E. Geach[1], C. Tremonti[2], A. M. Diamond-Stanic[3], P. H. Sell[4,5], A. A. Kepley[6], A. L. Coil[7], G. Rudnick[8], R. C. Hickox[9], J. Moustakas[10], and Yujin Yang[11]
[1] Centre for Astrophysics Research, School of Physics, Astronomy & Mathematics, University of Hertfordshire, Hatfield AL10 9AB, UK; j.geach@herts.ac.uk
[2] Department of Astronomy, University of Wisconsin-Madison, 475 North Charter Street, Madison, WI 53706, USA
[3] Department of Physics and Astronomy, Bates College, 44 Campus Avenue, Carnegie Science Hall, Lewiston, ME 04240, USA
[4] Foundation for Research and Technology-Hellas, 71110 Heraklion, Crete, Greece
[5] Physics Department & Institute of Theoretical & Computational Physics, University of Crete, 71003 Heraklion, Crete, Greece
[6] National Radio Astronomy Observatory, 520 Edgemont Road, Charlottesville, VA 22903, USA
[7] Center for Astrophysics and Space Sciences, Department of Physics, University of California, 9500 Gilman Drive, La Jolla, CA 92093, USA
[8] Department of Physics and Astronomy, The University of Kansas, Malott Room 1082, 1251 Wescoe Hall Drive, Lawrence, KS, 66045, USA
[9] Department of Physics and Astronomy, Dartmouth College, 6127 Wilder Laboratory, Hanover, NH 03755, USA
[10] Department of Physics and Astronomy, Siena College, 515 Loudon Road, Loudonville, NY 12211, USA
[11] Korea Astronomy and Space Science Institute, 776 Daedeokdae-ro, Yuseong-gu, Daejeon, 34055, Republic of Korea
Received 2018 July 19; revised 2018 July 25; accepted 2018 July 25; published 2018 August 23

Abstract

We present Atacama Large Millimeter/submillimeter Array observations of a massive ($M_\star \approx 10^{11}\,M_\odot$) compact ($r_{e,UV} \approx 100$ pc) merger remnant at $z = 0.66$ that is driving a 1000 km s^{-1} outflow of cool gas, with no observational trace of an active galactic nucleus (AGN). We resolve molecular gas on scales of approximately 1–2 kpc, and our main finding is the discovery of a wing of blueshifted CO $J(2 \rightarrow 1)$ emission out to -1000 km s^{-1} relative to the stars. We argue that this is the molecular component of a multiphase outflow, expelled from the central starburst within the past 5 Myr through stellar feedback, although we cannot rule out previous AGN activity as a launching mechanism. If the latter is true, then this is an example of a relic multiphase AGN outflow. We estimate a molecular mass outflow rate of approximately 300 $M_\odot$ yr^{-1}, or about one third of the 10 Myr-averaged star formation rate. This system epitomizes the multiphase "blowout" episode following a dissipational major merger—a process that has violently quenched central star formation and supermassive black hole growth.

Key words: galaxies: active – galaxies: evolution – galaxies: general – galaxies: starburst – ISM: kinematics and dynamics

1. Introduction

When accurate measurements of the mean baryon density of the universe were made ($\Omega_b \approx 0.04$, e.g., Spergel et al. 2003), it was quickly realized that the standard model of galaxy formation of the day (e.g., Rees & Ostriker 1977; White & Rees 1978; White & Frenk 1991; Somerville & Primack 1999) needed urgent revision. In particular, truncation, or at least dramatic modification, of the star formation histories of massive galaxies is required in models of galaxy formation (Benson et al. 2003; Granato et al. 2004; De Lucia et al. 2006) in order to reproduce the demographics of the galaxy population at $z = 0$ (e.g., Bower et al. 2006; Croton et al. 2006).

When star formation is curtailed more rapidly than what would be expected from normal consumption of the gas reservoir, we refer to this as "quenching." At its most extreme end, feedback from energy and momentum input to the interstellar medium might rapidly (within a few 10s Myr) shut down star formation on whole galaxy scales (Silk & Rees 1998). The most efficient means of achieving this is by rapidly destroying, or removing, molecular gas (Feruglio et al. 2010; Sturm et al. 2011; Bolatto et al. 2013; Veilleux et al. 2013; Cicone et al. 2014, 2018; Geach et al. 2014; Biernacki & Teyssier 2018). We refer to this process as "violent quenching." This is relevant not only to the star formation history of galaxies but also their chemical evolution, as it propels metal-enriched gas through galaxies and into the circumgalactic medium (Veilleux et al. 2013; Tumlinson et al. 2017; Baron et al. 2018).

In galaxy formation lore (e.g., Silk & Rees 1998; Di Matteo et al. 2005), feedback from active galactic nuclei (AGNs) is the standard route to quench massive galaxies, with quasar mode feedback capable of violent quenching through blowout (Hopkins & Elvis 2010). However, we have been studying a rare sample of massive ($M_\star \approx 10^{11}\,M_\odot$) compact galaxies at $z \approx 0.6$ driving ultrafast outflows of cool gas that appear to be driven by pure stellar feedback (Diamond-Stanic et al. 2012).

Our sample was selected from the Sloan Digital Sky Survey (SDSS; York et al. 2000) to have spectral features indicative of early-stage quenching. Subsequent follow-up observations revealed highly blueshifted ($\Delta V \approx -1000$ km s^{-1}) Mg II $\lambda\lambda$2796, 2804 Å interstellar absorption lines indicative of unusually fast ionized gas outflows (Tremonti et al. 2007). *Hubble Space Telescope* (*HST*) imaging reveals that the galaxies have incredibly compact optical morphologies with effective radii of $r_e \approx 100$ pc, and tidal features suggestive of late-stage major mergers (Sell et al. 2014). Their *WISE* 22 μm fluxes indicate high star formation rates (SFRs) and imply extreme SFR surface densities $\Sigma_{SFR} > 500\,M_\odot$ yr^{-1} kpc^{-2} (Diamond-Stanic et al. 2012), well in excess of what is required to launch such extreme winds (e.g., Murray et al. 2005). The majority of these systems present no clear evidence of an energetically dominant AGN (Sell et al. 2014), suggesting that stellar feedback could be driving the outflows.

Table 1
ALMA Observations of SDSS J1341−0321

Campaign	Cycle 4	Cycle 5
Dates of observation	2017 Mar 8	2017 Dec 30 2018 Jan 6, 7
Number of 12 m antennas	41	43–46
Baseline separation	15–331 m	15–2517 m
System temperature $\langle T_{sys} \rangle$	85.3 K	71.5 K
Mean pwv	4.8 mm	2.2 mm
Average elevation	61°	62°
Time on source	123 minutes	292 minutes
Atmospheric calibrators	J1337−1257 J1335−0511 Ganymede Titan	J1337−1257
Bandpass calibrators	J1337−1257	J1337−1257
Flux calibrators	Ganymede Titan	J1337−1257
Phase calibrators	J1335−0511	J1332−0509
Pointing calibrators	J1337−1257 J1742−1517 J1332−0509	J1337−1257

Geach et al. (2013, 2014) detected CO $J(2 \rightarrow 1)$ emission in two of the sample, revealing an implied global star formation efficiency close to the upper limit of Eddington-limited models of star formation (Murray et al. 2005; Thompson et al. 2015), and the presence of a high velocity CO $J(2 \rightarrow 1)$ wing, indicating a molecular outflow. In this Letter, we present new, more sensitive CO $J(2 \rightarrow 1)$ observations of another galaxy in the sample with the Atacama Large Millimeter/submillimeter Array (ALMA). We are able to resolve the CO $J(2 \rightarrow 1)$ on scales down to $0\farcs25$, allowing us to map the molecular gas on similar scales as the starlight. Throughout we assume a *Planck* 2015 cosmology, $h = H_0/100\ \mathrm{km\ s^{-1}\ Mpc^{-1}} = 0.677$, $\Omega_\mathrm{m} = 0.307$, $\Omega_\Lambda = 0.693$ (Planck Collaboration 2015).

2. Observations and Data Reduction

SDSS J1341−0321 ($z = 0.66$) at $\alpha = 13^\mathrm{h}41^\mathrm{m}36\fs80$, $\delta = -03°21'25\farcs3$ (J2000) was observed in ALMA Cycle 4 (2016.1.01072.S) and in Cycle 5 (2017.1.01318.S). The observations are summarized in Table 1.

We concatenate the calibrated Cycle 4 and 5 measurement sets in CASA (version 5.1.0) and image them using the *clean* command. To explore the morphology of the source we image the visibilities using natural and Briggs weighting, with robust parameter $R = 0$ for the latter. First we generate dirty maps in order to identify the CO $J(2 \rightarrow 1)$ emission and to evaluate the channel sensitivity. We then clean to a stopping threshold of 1σ, using a circular mask of radius $5''$ centered on the source (amply covering the emission). We employ multi-scale cleaning with four components corresponding to a delta function and Gaussians with widths of 1, 2, and 5× the synthesized natural beam, which has a FWHM of ($0\farcs42 \times 0\farcs32$) with position angle of 88°.

3. Analysis and Results

3.1. Optical and Near-infrared Imaging

In Figure 1 we present *HST* imaging of SDSS J1341−0321, revealing a compact central core with two faint tidal arms spanning several arcseconds. The target was observed with the Wide Field Camera 3 (WFC3) Ultraviolet Imaging Spectrograph (UVIS) channel using the F475W and F814W filters and the infrared (IR) channel using the F160W filter. All of the images were registered to one another with *tweakreg* to $\delta_\theta \approx 0\farcs01$ and then boresight-aligned to an SDSS (Albareti et al. 2017) overlapping field to the approximate astrometric precision of SDSS ($\delta_\theta \approx 0\farcs2$).

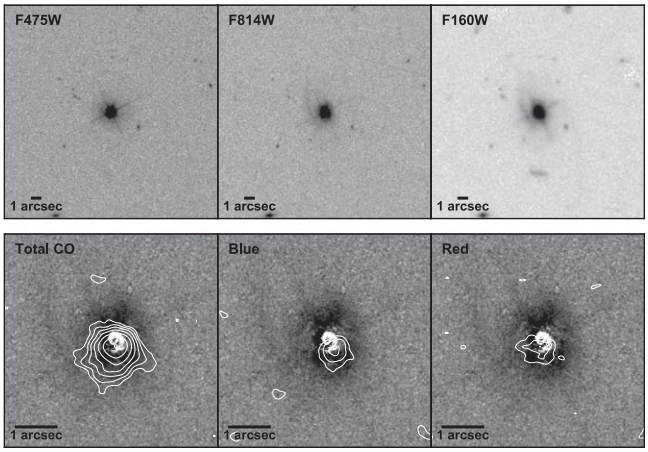

Figure 1. Top panels: *HST* WFC3 UVIS (F475W, F814W) and IR (F160W) images of SDSS J1341−0321 spanning $20''$. Two faint tidal tails are visible and extend over several arcseconds ($1'' \approx 7$ kpc), but the majority of the stellar emission is unresolved. Bottom panels: $5''$ zoom-ins showing the Sérsic model-subtracted F814W image (Section 3.2) as grayscale and CO $J(2 \rightarrow 1)$ contours, averaged over (left) $|\Delta V| < 1000\ \mathrm{km\ s^{-1}}$, (middle) $-1000 < \Delta V < -500\ \mathrm{km\ s^{-1}}$, (right) $500 < \Delta V < 1000\ \mathrm{km\ s^{-1}}$. CO $J(2 \rightarrow 1)$ contours start at 3σ and are logarithmically spaced at 0.2 dex multiples of σ. All images are orientated north up, east is left. Note that the absolute astrometric precision of the *HST* images (boresight-aligned to SDSS) is $\delta_\theta \approx 0\farcs2$.

Like most other galaxies in our sample, SDSS J1341−0321 is extremely compact. When quantifying the compactness with GALFIT (version 3; Peng et al. 2010), we focus on the F475W and F814W bands, which have the best spatial resolution (FWHM $\approx 0\farcs07$), and we find $r_{\mathrm{e,UV}} \simeq 100$, 110 pc based on single-component Sérsic models with $n = 4$. Further details on image processing and morphological analysis can be found in Sell et al. (2014).

3.2. Optical Spectroscopy and Stellar Population Modeling

Figure 2 presents the rest-frame UV–optical spectrum of SDSS J1341−0321 obtained with the *Magellan* Echellette (MagE) spectrograph (Marshall et al. 2008) on the *Magellan* Clay telescope with a $1''$ slit and 2 hr of integration time. The data were reduced and calibrated using the *MASE* pipeline (Bochanski et al. 2009). The spectrum has a resolution $R \sim 4100$ over a bandpass of 3300–9400 Å and a signal-to-noise of ∼45 per resolution element near the galaxy's Mg II $\lambda\lambda$2796,2804 Å absorption lines. The spectrum displays a very blue UV–optical continuum with weak stellar Balmer absorption lines, suggesting a stellar population dominated by O and B stars. The Mg II and Fe II (λ2344, 2374, 2383, 2587 and 2600 Å) interstellar medium (ISM) absorption lines are highly blueshifted relative to the stars (insets). The presence of two sets of absorption profiles for each species implies two distinct velocity components at roughly -500 and $-1000\ \mathrm{km\ s^{-1}}$, indicating two potential outflow events.

Could the central unresolved emission, blue and nearly featureless continuum, and moderately broad Hβ emission line

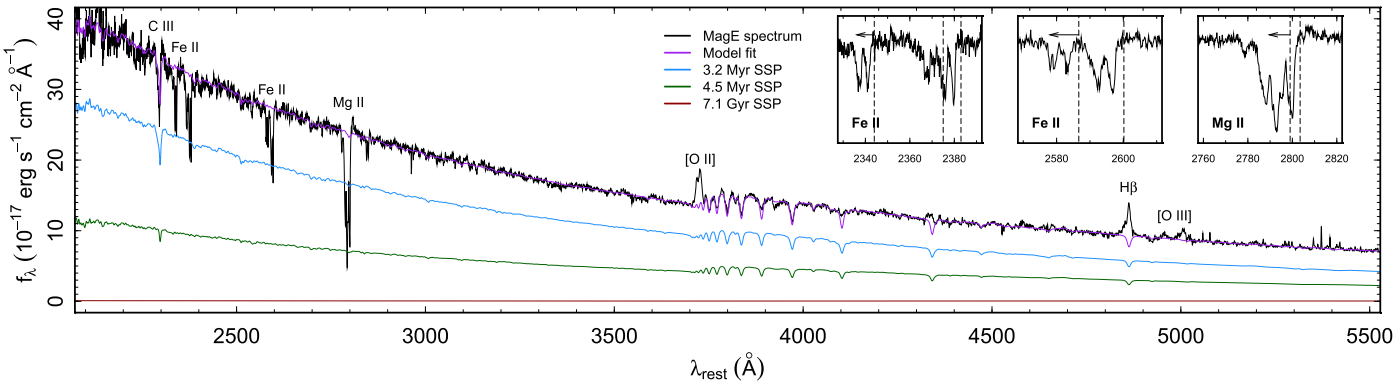

Figure 2. *Magellan* Echellette (MagE) optical spectrum of SDSS J1341−0321 in the rest-frame. We show the best-fitting model from our simple stellar population (SSP) modeling (Section 3.2) illustrating that the stellar continuum emission is dominated by very young ($t < 5$ Myr) populations. The redshift $z = 0.6611$ is determined from the stellar absorption lines. The inset panels show zoom-ins of the model continuum normalized spectrum around the Fe II λ2344, 2374, 2383, 2587, and 2600 Å and Mg II $\lambda\lambda$2796, 2804 Å ISM absorption lines. Vertical dashed lines indicate the rest-frame wavelengths of the lines, and the arrows indicate a blueshift vector of -1000 km s^{-1}. Note that the 7.1 Gyr component is so weak relative to the young populations that it appears almost featureless in this plot.

be due to the presence of an unobscured (Type I) AGN? The continuum is very well fit by stellar population models, as shown in Figure 2, and the presence of a strong C III λ2298 Å P Cygni absorption feature indicates a dominant population of Wolf–Rayet stars (Leitherer et al. 2014). The Hβ emission line is noticeably broadened ($\sigma \sim 600$ km s^{-1}); however, it is not as broad as the Hβ lines found in Type I AGNs (>1000 km s^{-1}; Osterbrock & Mathews 1986; Sulentic et al. 2000). We hypothesize that some of the Hβ emission arises in the outflow itself (see Figure 4). The [O II] $\lambda\lambda$3726,3729Å line is also dominated by a broad component that could trace the outflow; this line is typically narrow in Type I AGN.

Could SDSS J1341−0321 host an obscured (Type II) AGN? We combine the MagE spectrum with Keck/Near-Infrared Spectrograph (NIRSpec) data covering the [N II] λ6584 Å and Hα lines (E. George et al. 2018, in preparation), decomposing the lines into broad (∼600 km s^{-1}) and narrow (∼200 km s^{-1}) components, and place them on the Baldwin et al. (1981) "BPT" AGN diagnostic diagram. Both the narrow and broad components of the emission lines fall in the "composite" region (Kewley et al. 2006), likely due to the contribution of shocks associated with the merger and outflow (Ho et al. 2014; Rich et al. 2014). Notably, the narrow component lies very close to the star formation divider line when the latter is adjusted for redshift (Kewley et al. 2013). Finally, the galaxy's *WISE* (Wright et al. 2010) $W1 - W2$ color is 0.258 ± 0.005, well below the AGN selection threshold of Stern et al. (2012) ($W1 - W2 > 0.8$) and the more conservative threshold recommended by Blecha et al. (2018; $W1 - W2 > 0.5$). We conclude that SDSS J1341−0321 is unlikely (currently) to host an AGN.

We fit the spectrum with a combination of simple stellar population (SSP) models and a Calzetti et al. (2000) reddening law. We employed the Flexible Stellar Population Synthesis code (Conroy et al. 2009; Conroy & Gunn 2010) to generate SSPs with Padova 2008 isochrones, a Salpeter (1955) initial mass function (IMF), and a new theoretical stellar library "C3K" (C. Conroy et al. 2018, in preparation) with a resolution of $R \sim 10{,}000$. We utilize solar metallicity SSP templates with 43 ages spanning 1 Myr–8.9 Gyr. We perform the fit with the Penalized Pixel-Fitting (pPXF) software (Cappellari & Emsellem 2004; Cappellari 2017). The best-fit model is dominated by very young stellar populations, with approximately 87% of the continuum emission at 5500 Å contributed by populations less than 5 Myr old. The 10 Myr-averaged SFR inferred from the SSP modeling is $M_\odot \approx 900\, M_\odot$ yr^{-1}, after converting to a Chabrier IMF (Chabrier 2003).

Given the youth of the stellar population ($t < 5$ Myr), the nebular emission lines appear surprisingly weak. The Hβ equivalent width is 10 Å, a factor of ∼4 lower than SDSS galaxies with comparable colors and redshift. This is not an artifact of differential attenuation, for the stars and the gas have comparable reddening. One possibility is that the compact starburst has an unusually high ionization parameter. This would result in Lyman continuum photons penetrating deeply into the surrounding nebula and potentially being absorbed by dust before ionizing hydrogen atoms. Another possibility is that the outflow blew away much of the natal nebula on a short timescale, allowing ionizing photons to escape from the center of the galaxy. Notably, the Mg II and Fe II lines show no absorption near zero velocity, suggesting that the bulk of the ionized gas in the galaxy is outflowing.

3.3. CO $J(2 \rightarrow 1)$ Emission

Figure 1 presents the line-integrated CO $J(2 \rightarrow 1)$ emission in comparison to the *HST* imaging and Figure 3 shows the CO $J(2 \rightarrow 1)$ velocity-averaged maps in 333 km s^{-1}-wide channels, spanning $|\Delta V| \lesssim 1500$ km s^{-1} around the systemic redshift of the galaxy. Figure 4 shows the total CO $J(2 \rightarrow 1)$ spectrum. The integrated line flux is $S_{\rm CO}\Delta V = 3.4 \pm 0.1$ Jy km s^{-1}, corresponding to a luminosity of $L'_{\rm CO} = (2.0 \pm 0.1) \times 10^{10}$ K km s^{-1} pc^2.

There is strong CO $J(2 \rightarrow 1)$ emission out to $\Delta V \approx \pm 300$ km s^{-1} relative to the stars (including an inner spiral or tidal arm visible on the receding side), as well as a significant wing to $\Delta V \approx -1000$ km s^{-1}. In Figure 4 we show on the same velocity scale the continuum-subtracted Fe II and Mg II absorption lines and the Hβ and [O II] nebular emission lines. The nebular and absorption lines extend to similar blueshifted velocities as seen in CO $J(2 \rightarrow 1)$ emission, implying that they could all be tracing the same outflowing gas.

The CO $J(2 \rightarrow 1)$ morphology is complex; in the naturally weighted image, the peak of the emission within a few 100 km s^{-1} of the systemic is (a) not coincident with the peak of the starlight, and (b) elongated roughly S–W. A Briggs weighting of the visibilities allows us to examine the central CO $J(2 \rightarrow 1)$ morphology in more detail by tailoring

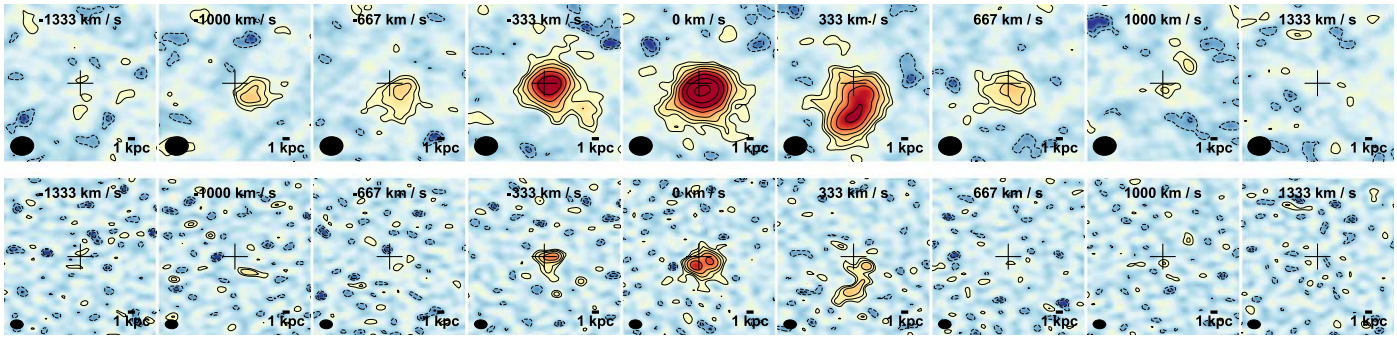

Figure 3. CO $J(2 \rightarrow 1)$ maps of SDSS J1341−0321 averaged over 333 km s^{-1} channels spanning $\Delta V = \pm$ 1500 km s^{-1} (labels give channel centers) relative to the systemic redshift. The top row shows the naturally weighted images, and the bottom row shows the Briggs ($R = 0$) weighted images. Contours start at 2σ and are logarithmically spaced at 0.2 dex multiples of σ. Dashed contours are negative equivalents. The crosshair indicates the peak of the stellar emission in the *HST*/F814W imaging (Figure 1). Black ellipses show the FWHM of the synthesized beam.

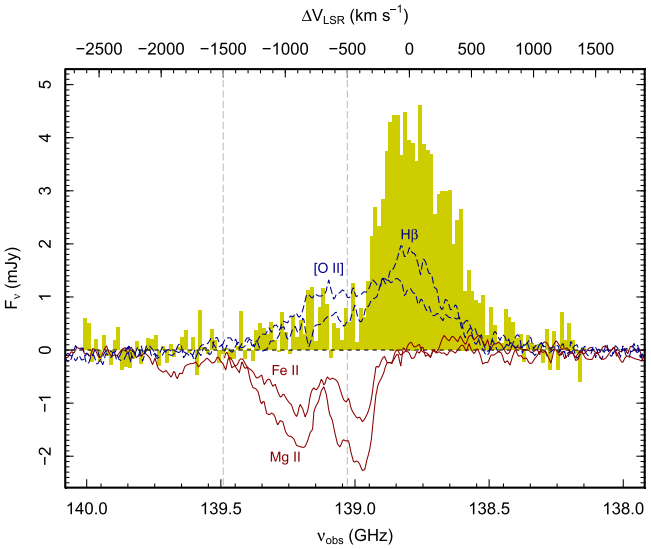

Figure 4. Total CO $J(2 \rightarrow 1)$ spectrum of SDSS J1341−0321, summed over the 3σ contour of the zeroth moment image. We also show the continuum-subtracted MagE Hβ, [O II], Fe II λ2600 Å, and Mg II lines on the same velocity scale. The two lines of the Mg II doublet are separated by 770 km s^{-1}, but the maximum outflow velocity is larger than this value, causing some line profile blending. We crudely deblend the Mg II doublet by showing the profile of the redder line (2804 Å) at $\Delta V > -770$ km s^{-1} and the profile of the bluer line (2796 Å) at $\Delta V < -770$ km s^{-1}. We deblend the [O II] doublet in a similar manner, but the closer spacing of the two lines ($\Delta V = 222$ km s^{-1}) means that there is still some velocity overlap. The Fe II and Hβ lines do not suffer from blending. Significant CO $J(2 \rightarrow 1)$ emission extends to at least $\Delta V \approx -1000$ km s^{-1}, similar to the nebular lines. There are at least two distinct velocity components seen in the absorption lines. Vertical dashed lines indicate the velocity range we consider to be outflowing molecular gas.

the "robust" parameter R to produce a smaller synthesized beam, albeit at the expense of sensitivity, such that we only detect CO $J(2 \rightarrow 1)$ emission within $\Delta|V| \lesssim 350$ km s^{-1}. With $R = 0$ we can image the CO $J(2 \rightarrow 1)$ emission at a resolution of ($0\farcs25 \times 0\farcs18$). Interestingly, at this resolution the emission at zero velocity has a double lobed morphology, straddling the bright peak of the stellar emission. This suggests that the bulk of the molecular gas close to zero velocity is not coincident with the site of very recent intense star formation. We postulate that we are seeing the blue starburst though a relatively low obscuring column—a result of ISM blowout.

4. Interpretation

SDSS J1341−0321 is clearly a late-stage merger, with obvious tidal features in the extended stellar emission, and so it is reasonable to conclude that some of the dynamical structure in the CO $J(2 \rightarrow 1)$ emission is associated with dense interstellar material dispersed by tidal forces. Indeed, as evident in the channel maps (Figure 3), there is a prominent CO $J(2 \rightarrow 1)$ feature located at $\Delta V \approx 300$ km s^{-1}, describing an arc of molecular emission that is roughly co-spatial with the inner part of a spiral or tidal arm visible in the *HST* imaging. However, the CO $J(2 \rightarrow 1)$ emission at -1000 km s^{-1} cannot plausibly be associated with purely tidal debris resulting from the merger; we argue that it is more likely to have been propelled to high velocity as part of a multiphase outflow driven by the starburst.

4.1. Violent Quenching

We estimate the molecular mass outflow rate assuming a time-averaged thin shell approximation (Rupke et al. 2005), where CO $J(2 \rightarrow 1)$ is tracing outflowing H_2 with total mass $M_{H_2,out}$ in a shell of radius R_{out}, traveling at v_{out}: $\dot{M}_{H_2,out} = v_{out} M_{H_2,out} / R_{out}$. To estimate $M_{H_2,out}$ we only consider emission between -500 and -1500 km s^{-1} and assume the optically thin case appropriate for a turbulent outflow $M_{H_2} = 0.34 L'_{CO}$ (Bolatto et al. 2013). Obviously the choice of α_{CO} will have a systematic effect on the derived mass outflow rate: increasing it will increase $\dot{M}_{H_2}$. We further assume that the CO $J(2 \rightarrow 1)$ emission is thermalized, which is also a conservative assumption because a correction for sub-thermal excitation will also drive up the mass estimate.

Another key uncertainty is the geometry of the outflowing gas. At $\Delta V \approx -1000$ km s^{-1} the peak of the CO $J(2 \rightarrow 1)$ emission is offset (0.28 ± 0.02)″ from the peak of the CO $J(2 \rightarrow 1)$ emission measured at zero velocity, corresponding to a projected distance of (2.0 ± 0.1) kpc, similar to the distance covered by a parcel of gas traveling at 500–1000 km s^{-1} for 3 Myr, and so we take it as reasonable estimate of R_{out}. We fully acknowledge that poor constraints on the wind geometry are a major systematic uncertainty in the calculation. The final consideration is the choice of v_{out}. The observed CO $J(2 \rightarrow 1)$ velocities are subject to projection effects. One approach is to take the maximum velocity in the wing as the deprojected velocity of the outflow (e.g., Maiolino et al. 2012); however, this could potentially dramatically overestimate the outflow rate. We take a conservative approach and do not deproject the

velocities, and instead integrate over the spectrum such that

$$\dot{M}_{\rm H_2,out} \propto \int_{-1500\ {\rm km\ s^{-1}}}^{-500\ {\rm km\ s^{-1}}} vS_\nu dv \quad (1)$$

This gives $\dot{M}_{\rm H_2,out} = 310 \pm 70\, M_\odot\, {\rm yr}^{-1}$, implying a mass loading factor of $\eta \sim 1/3$ given the 10 Myr-averaged SFR.

The corresponding kinetic power of the outflow (integrating similarly over the wing) is $P_{\rm k} = v^2 \dot{M}_{\rm H_2,out}/2$, yielding $P_{\rm k} = (0.8 \pm 0.3) \times 10^{44}$ erg s^{-1}, or approximately 1% of the bolometric luminosity (see Feruglio et al. 2010), with $\log_{10}(L_{\rm IR}/{\rm erg\ s^{-1}}) = 46.0$ based on the integrated $\lambda_{\rm rest} =$ 8–1000 μm Chary & Elbaz (2001) template fits to the *WISE* 12 and 22 μm flux (Diamond-Stanic et al. 2012). The momentum flux in the molecular gas is $\dot{p} = v\dot{M}_{\rm H_2}$, with $\dot{p} = (1.8 \pm 0.5) \times 10^{36}$ dyne. The total momentum input from the recent starburst, L/c, is approximately 8×10^{35} dyne, which seems insufficient to drive the outflow, assuming a momentum-conserving wind. However, allowing for multiple scatterings, additional momentum contributions from supernovae, uncertainties on the wind geometry (particularly the radius), and $\alpha_{\rm CO}$ could bring the values to parity. As there is likely to be additional mass and momentum in the warm and hot phases of the outflow, the momentum budget remains tight. It is possible that the outflow could have been launched by a past AGN that now leaves no observational trace.

Regardless of the launching mechanism, the high mass outflow rate in molecular gas, young unobscured central starburst remnant, and lack of present AGN indicates that the core of this galaxy has been violently quenched, curtailing both stellar mass and supermassive black hole growth.

5. Conclusions and Closing Remarks

Explaining the survival of cold–cool[12] gas in fast galaxy scale winds has traditionally been a struggle for simulations, and the presence of cold molecular gas at first glance exacerbates this issue. Radiative driving was originally proposed as an attractive mechanism to propel cold gas to large galactocentric radius because it favors the survival of cold–cool clouds compared to ram pressure driving (Murray et al. 2005; Thompson et al. 2015), although multiple driving mechanisms are expected to be required to produce a multiphase wind. However, rather than being directly expelled, cool, and even cold, gas could condense out of a hot wind. Schneider et al. (2018) presented hydrodynamic simulations demonstrating that, when radiative cooling is included, a hot, mass-loaded ($\eta \approx 0.5$) outflow can produce cool (10^4 K) gas with $v_{\rm out} \approx 1000\ {\rm km\ s^{-1}}$, but the cooling floor in these simulations precludes an analysis of any molecular component. Through an analytic approach, Zubovas & King (2014) argued that *molecular* gas can cool out of a hot (AGN shock-driven) wind, and in hydro-chemical simulations Richings & Faucher-Giguére 2018a, 2018b also demonstrated that molecular outflows can form via in situ cooling within AGN-driven winds.

Relevant to this work, Zubovas & King propose that 1000 km s^{-1} cold–cool gas outflows *always* have an AGN origin even in cases—like this—where an AGN is not visible, as the wind signature is visible for some 10s of Myr after the central engine switches off. Given the tension between the energetics of the molecular outflow and the energy budget of the recent starburst, we leave open the possibility that SDSS J1341−0321—and possibly other galaxies in our sample—presents an example of a relic AGN outflow. Nevertheless, we conclude by remarking on this galaxy's extraordinarily high implied star formation surface density of $\Sigma_{\rm SFR} \approx 30{,}000\, M_\odot\, {\rm yr}^{-1}\, {\rm kpc}^{-2}$, and maintain that momentum injection by compact starbursts triggered during major mergers can be a competitive mechanism to quench the centers of massive galaxies.

[12] I.e., molecular, atomic and ionized gas with $T < 10^4$ K.

We thank the anonymous referee for a constructive report that helped improve this work. We also thank Tim Heckman for useful discussions and Charlie Conroy for providing his C3K models prior to publication. J.E.G. is supported by the Royal Society. G.R. would like to thank the University of Hamburg Observatory and the European Southern Observatory (ESO) for their hospitality in hosting him while working on this paper. G.R. would additionally like to thank ESO for financial support through their scientific visitor program. The National Radio Astronomy Observatory is a facility of the National Science Foundation operated under cooperative agreement by Associated Universities, Inc. R.C.H. acknowledges support from the National Science Foundation through CAREER grant No. 1554584. The authors acknowledge excellent support of the UK ALMA Regional Centre Node. This Letter makes use of the following ALMA data: 2016.1.01072.S, 2017.1.0318.S. ALMA is a partnership of ESO (representing its member states), NSF (USA), and NINS (Japan), together with NRC (Canada) and NSC and ASIAA (Taiwan), in cooperation with the Republic of Chile. The Joint ALMA Observatory is operated by ESO, AUI/NRAO, and NAOJ. Support for HST-GO-12272, HST-GO-13689, and HST-GO-14239 was provided by NASA through a grant from the Space Telescope Science Institute, which is operated by the Association of Universities for Research in Astronomy, Incorporated, under NASA contract NAS5-26555.

ORCID iDs

J. E. Geach https://orcid.org/0000-0003-4964-4635
C. Tremonti https://orcid.org/0000-0003-3097-5178
P. H. Sell https://orcid.org/0000-0003-1771-5531
A. A. Kepley https://orcid.org/0000-0002-3227-4917
A. L. Coil https://orcid.org/0000-0002-2583-5894
G. Rudnick https://orcid.org/0000-0001-5851-1856
R. C. Hickox https://orcid.org/0000-0003-1468-9526
J. Moustakas https://orcid.org/0000-0002-2733-4559
Yujin Yang https://orcid.org/0000-0003-3078-2763

References

Albareti, F. D., Allende Prieto, C., Almeida, A., et al. 2017, ApJS, 233, 25
Baldwin, J. A., Phillips, M. M., & Terlevich, R. 1981, PASP, 93, 5
Baron, D., Netzer, H., Prochaska, J. X., et al. 2018, MNRAS, in press, doi:10.1093/mnras/sty2113
Benson, A. J., Bower, R. G., Frenk, C. S., et al. 2003, ApJ, 599, 38
Biernacki, P., & Teyssier, R. 2018, MNRAS, 475, 5688
Blecha, L., Snyder, G. F., Satyapal, S., & Ellison, S. L. 2018, MNRAS, 478, 3056
Bochanski, J. J., Hennawi, J. F., Simcoe, R. A., et al. 2009, PASP, 121, 1409
Bolatto, A. D., Warren, S. R., Leroy, A. K., et al. 2013, Natur, 499, 450
Bower, R. G., Benson, A. J., Malbon, R., et al. 2006, MNRAS, 370, 645
Calzetti, D., Armus, L., Bohlin, R. C., et al. 2000, ApJ, 533, 682
Cappellari, M. 2017, MNRAS, 466, 798
Cappellari, M., & Emsellem, E. 2004, PASP, 116, 138
Chabrier, G. 2003, PASP, 115, 763

Chary, R., & Elbaz, D. 2001, ApJ, 556, 562
Cicone, C., Maiolino, R., Sturm, E., et al. 2014, A&A, 562, A21
Cicone, C., Severgnini, P., Papadopoulos, P. P., et al. 2018, arXiv:180706015C
Conroy, C., & Gunn, J. E. 2010, ApJ, 712, 833
Conroy, C., Gunn, J. E., & White, M. 2009, ApJ, 699, 486
Croton, D. J., Springel, V., White, S. D. M., et al. 2006, MNRAS, 365, 11
De Lucia, G., Springel, V., White, S. D. M., Croton, D., & Kauffmann, G. 2006, MNRAS, 366, 499
Diamond-Stanic, A. M., Moustakas, J., Tremonti, C. A., et al. 2012, ApJL, 755, L26
Di Matteo, T., Springel, V., & Hernquist, L. 2005, Natur, 433, 604
Feruglio, C., Maiolino, R., Piconcelli, E., et al. 2010, A&A, 518, L155
Geach, J. E., Hickox, R. C., Diamond-Stanic, A. M., et al. 2013, ApJL, 767, L17
Geach, J. E., Hickox, R. C., Diamond-Stanic, A. M., et al. 2014, Natur, 516, 68
Granato, G. L., De Zotti, G., Silva, L., Bressan, A., & Danese, L. 2004, ApJ, 600, 580
Ho, I.-T., Kewley, L. J., Dopita, M. A., et al. 2014, MNRAS, 444, 3894
Hopkins, P. F., & Elvis, M. 2010, MNRAS, 401, 7
Kewley, L. J., Groves, B., Kauffmann, G., & Heckman, T. 2006, MNRAS, 372, 961
Kewley, L. J., Maier, C., Yabe, K., et al. 2013, ApJL, 774, L10
Leitherer, C., Ekström, S., Meynet, G., et al. 2014, ApJS, 212, 14
Maiolino, R., Gallerani, S., Neri, R., et al. 2012, MNRAS, 425, L66
Marshall, J. L., Burles, S., Thompson, I. B., et al. 2008, Proc. SPIE, 7014, 701454
Murray, N., Quataert, E., & Thompson, T. A. 2005, ApJ, 618, 569
Osterbrock, D. E., & Mathews, W. G. 1986, ARA&A, 24, 171
Peng, C. Y., Ho, L. C., Impey, C. D., & Rix, H.-W. 2010, AJ, 139, 2097
Planck Collaboration 2015, A&A, 594, A13
Rees, M. J., & Ostriker, J. P. 1977, MNRAS, 179, 541
Rich, J. A., Kewley, L. J., & Dopita, M. A. 2014, ApJL, 781, L12
Richings, A. J., & Faucher-Giguére, C.-A. 2018a, MNRAS, 474, 3673
Richings, A. J., & Faucher-Giguére, C.-A. 2018b, MNRAS, 478, 3100
Rupke, D. S., Veilleux, S., & Sanders, D. B. 2005, ApJS, 160, 115
Salpeter, E. E. 1955, ApJ, 121, 161
Schneider, E. E., Robertson, B. E., & Thompson, T. A. 2018, arXiv:1803.01005
Sell, P. H., Tremonti, C. A., Hickox, R. C., et al. 2014, MNRAS, 441, 3417
Silk, J., & Rees, M. J. 1998, A&A, 331, L1
Somerville, R. S., & Primack, J. R. 1999, MNRAS, 310, 1087
Spergel, D. N., Verde, L., Peiris, H. V., et al. 2003, ApJS, 148, 175
Stern, D., Assef, R. J., Benford, D. J., et al. 2012, ApJ, 753, 30
Sturm, E., González-Alfonso, E., Veilleux, S., et al. 2011, ApJL, 733, L16
Sulentic, J. W., Marziani, P., & Dultzin-Hacyan, D. 2000, ARA&A, 38, 521
Thompson, T. A., Fabian, A. C., Quataert, E., & Murray, N. 2015, MNRAS, 449, 147
Tremonti, C. A., Moustakas, J., & Diamond-Stanic, A. M. 2007, ApJL, 663, L77
Tumlinson, J., Peeples, M. S., & Werk, J. K. 2017, ARA&A, 55, 389
Veilleux, S., Meléndez, M., Sturm, E., et al. 2013, ApJ, 776, 27
White, S. D. M., & Frenk, C. S. 1991, ApJ, 379, 52
White, S. D. M., & Rees, M. J. 1978, MNRAS, 183, 341
Wright, E. L., Eisenhardt, P. R. M., Mainzer, A. K., et al. 2010, AJ, 140, 1868
York, D. G., Adelman, J., Anderson, J. E., Jr., et al. 2000, AJ, 120, 1579
Zubovas, K., & King, A. R. 2014, MNRAS, 439, 400